JOURNAL OF Materials CHEMISTRY

Preparation of metallic BEDT-TTF charge transfer complex of 3,3′,5,5′-tetranitro-4,4′-biphenyldiol dianion ($TNBP^{2-}$) having flexible molecular shape†

Kazukuni Nishimura,*[a] Tetsuo Kondo,[a,b] Olga O. Drozdova,[a]‡ Hideki Yamochi[a,b] and Gunzi Saito*[a]

[a]*Division of Chemistry, Graduate School of Science, Kyoto University, Sakyo-ku, Kyoto 606-8502, Japan. E-mail: nishimura@kuchem.kyoto-u.ac.jp, saito@kuchem.kyoto-u.ac.jp*
[b]*CREST, Japan Science and Technology Corporation (JST), Japan*

Received 27th September 1999, Accepted 20th December 1999
Published on the Web 29th February 2000

Two kinds of 3,3′,5,5′-tetranitro-4,4′-biphenyldiol dianion ($TNBP^{2-}$) molecules having different dihedral angles (φ) between the two phenyl rings exist in the tetrabutylammonium salt of $TNBP^{2-}$ ($\varphi = 0°$ and 35°), while only one kind of $TNBP^{2-}$ molecule exists in the tetraphenylphosphonium salt ($\varphi = 0°$). The 4 : 1 cation radical salt of BEDT-TTF (ET) with $TNBP^{2-}$ as a counter anion is metallic down to 3 K. The ET molecules form a two-dimensional conducting layer which is sandwiched by the layers of flat $TNBP^{2-}$ molecules ($\varphi = 0°$). The crystal structure indicates the β''_{432}-type stacking of tetramerized ET molecules which is caused by hydrogen bonds between the CH groups of ET and the oxygen atoms (nitro and phenol) of $TNBP^{2-}$. The optical spectra in a KBr pellet are consistent with both the highly conductive and distorted structural nature. The magnetic susceptibility at room temperature is high ($\chi = 6.7 \times 10^{-4}$ emu spin^{-1}) compared with the conventional organic metal based on ET ($\chi = 3.4$–5.5×10^{-4} emu spin^{-1}) indicating strong electron correlation in the 4 : 1 complex. The temperature dependence of the magnetic susceptibility suggests a semimetallic nature which is consistent with the calculated Fermi surface. The calculated band width is comparable to the estimated effective on-site Coulomb repulsive energy. A semiconductive behavior with high conductivity is observed in the nearly 2 : 1 ET complex of $TNBP^{2-}$. A partial charge transfer state of the ET molecules is supported by the optical spectra. The high conductivity and optical data suggest that the 2 : 1 salt is not $(ET^{1+})_2(TNBP^{2-})$ but most plausibly $(ET^{0.5+})_2(HTNBP^{1-})$.

1 Introduction

The 3,3′,5,5′-tetranitro-4,4′-biphenyldiol molecule (H_2TNBP) is a multifunctional molecule (Fig. 1) capable of behaving both as a weak electron acceptor in the formation of charge transfer (CT) complexes and as a dibasic Brönsted acid in the formation of proton transfer (PT) complexes. The reduction peak potential of H_2TNBP is $E = -0.56$ V (*vs.* SCE (saturated calomel electrode), CH_3CN) which indicates the fairly weak electron accepting ability of H_2TNBP. H_2TNBP is also a rather strong Brönsted acid and has a pK_{a1} value of 4.90 in methanol or 3.86 in acetone–water (1 : 1). As a consequence a variety of neutral CT or ionic PT complexes of H_2TNBP have been prepared using aromatic hydrocarbons, aromatic amines and diamines, azines, bis(ethylenedioxy)tetrathiafulvalene (BEDO-TTF) and bis(ethylenedioxy)dibenzotetrathiafulvalene (BEDO-DBTTF) (Fig. 2, **I** and **II**).[1,2] Among them the *o*-dianisidine molecule has afforded two isomeric complexes, of which one is a black CT complex and the other is a yellow-to-orange PT complex.[1] Furthermore, a number of CPT type complexes, in which the CT and PT interactions operate simultaneously (Fig. 2, **III**), have been obtained using aromatic amines and diamines.[1]

In this paper a different kind of complex, *i.e.* a cation radical salt of BEDT-TTF (ET), which has provided a number of organic metals and superconductors,[3] is described using $TNBP^{2-}$ as counter dianion, produced by losing two protons from H_2TNBP (Fig. 2, **IV**–**VI**).

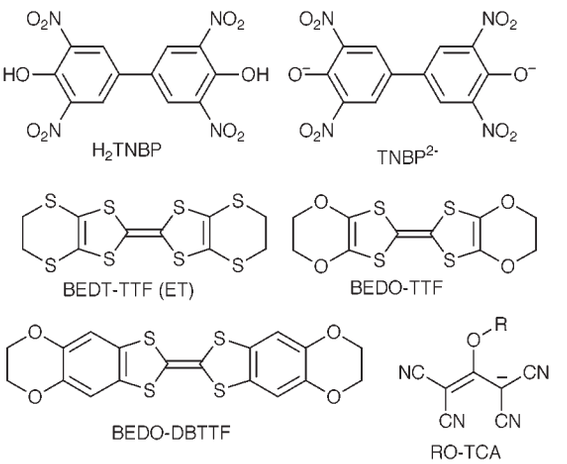

Fig. 1 Chemical structures of molecules discussed in the text.

†Crystal data, including bond lengths and angles and atomic coordinates and thermal parameters for $(TBA)_2(TNBP)$, $(Ph_4P)_2(TNBP)$ and $(ET)_4(TNBP)$ are available as supplementary data. For direct electronic access see http://www.rsc.org/suppdata/jm/a9/a907746d

‡Permanent address: A. F. Ioffe, Physco-Technical Institute, Russian Academy of Science, St. Petersburg, Russia.

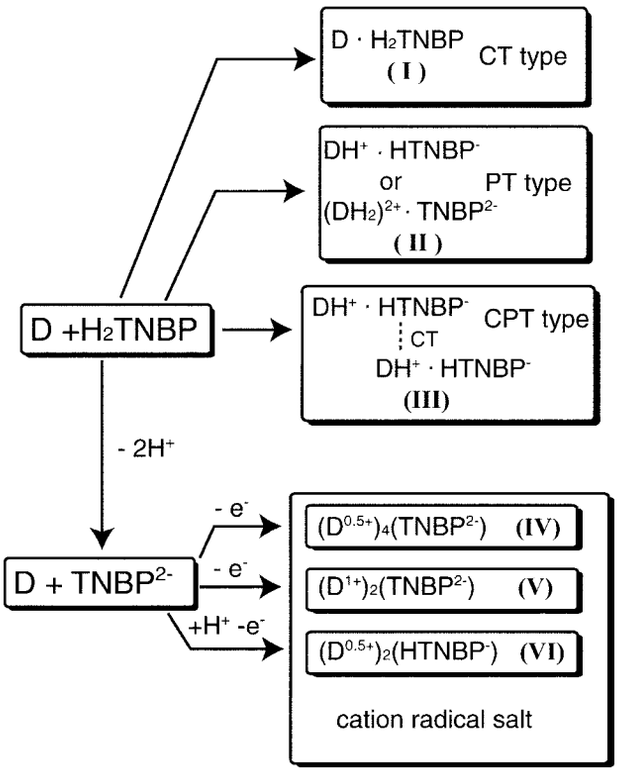

Fig. 2 Formation of complexes between D (electron donor and/or proton acceptor) and H_2TNBP (electron acceptor and/or proton donor). **I**: CT type, **II**: PT type, **III**: CPT type, **IV**, **V**, **VI**: cation radical salt.

2 Experimental

Preparation of terabutylammonium (TBA), tetraphenylphosphonium (Ph_4P) and BEDT-TTF (ET) salts of $TNBP^{2-}$

H_2TNBP was prepared by treating 4,4′-biphenyldiol with excess conc. HNO_3 in acetic acid at 95 °C (yield 75.6%, mp 224.4–224.7 °C).[4] H_2TNBP was treated with $NaNO_2$ in methanol to afford the disodium salt of $TNBP^{2-}$ in 87.5% yield, which was converted to TBA salt by TBA·Br in water (yield 98.4%, reddish purple, plates, mp 228.0–228.8 °C). $(TBA)_2(TNBP)$ did not exhibit an oxidation peak up to +1.80 V *vs.* SCE indicating that the dianion state is very stable. By using Ph_4P·Br instead of TBA·Br, the Ph_4P salt of $TNBP^{2-}$ was obtained (reddish purple needles, mp 264.9–265.1 °C).

Two kinds of ET salts were harvested by the electrooxidation of ET in the presence of $(TBA)_2TNBP$ from THF–ethanol or 1,1,2-trichloroethane (TCE). One of them was obtained as platelets $1 \times 1 \times 0.05$ mm^3 in size either from THF–ethanol or TCE as a minor product. Occasionally the platelet crystals coexist with very small amounts of powders. The platelet phase was found to be a 4 : 1 stoichiometry by elemental (calc. C 32.82, H 1.91, N 2.94, O 8.41; obs. C 32.80, H 2.01, N 2.66, O 8.66%), structural and density analyses.

The powders were found to be other kinds of ET salt. The powder phase was a major product and no contamination by the platelet phase was observed in most batches of powder phase. By using Na_2TNBP–18-crown-6 ether as an electrolyte, only the powder phase was obtained. The elemental analysis indicated nearly 2 : 1 stoichiometry for this phase: calc. C 33.91, H 1.78, N 4.94, O 14.11, S 45.26; obs. C 34.25, H 1.87, N 4.46, O 13.83, S 45.40%.

The platelet and powder phases are tentatively represented as $(ET)_4(TNBP)$ and $(ET)_2(TNBP)$, respectively.

Measurements

Melting points were not corrected. Cyclic voltammetry was performed in 0.1 M solutions of $TBA{\cdot}BF_4$ in CH_3CN with Pt electrodes *vs.* SCE at a scan speed of 10–20 mV s^{-1} using Yanaco Polarographic Analyzer P-1100 at 20–22 °C. Optical measurements were carried out with a KBr disk on a Perkin-Elmer Paragon 1000 Series FT-IR (resolution 4 cm^{-1}) for IR and near-IR regions (400–7800 cm^{-1}) and on Shimadzu UV-3100 spectrometer for near-infrared, visible and ultraviolet (UV–VIS–NIR) regions (3800–42 000 cm^{-1}). Dc conductivities were measured based on a standard two- or four-probe technique attaching gold wires (15–25 μm diameter) on samples with gold paste (Tokuriki 8560-1A). Static magnetic susceptibility measurements were done by the aid of SQUID magnetosusceptometer (Quantum Design MPMS) from 300 K to 2 K. EPR measurements were performed on a continuous wave X band EPR spectrometer (JEOL JES-TE200) with an Oxford TE_{011} cavity whose temperature was varied from RT to 3 K by means of the Oxford ESR-900 cryostat.

The stoichiometries of complexes were determined by elemental analysis, crystal structure analysis and/or density measurements of single crystals. The densities of crystals were determined by the floating method in a mixture of carbon tetrachloride and 1,2-dibromoethane or 1,1,2,2-tetrabromoethane. The intensity data of the structural analysis were collected in an automatic four circle diffractometer (MAC Science MXC$^{\chi}$) or oscillator type X-ray imaging plate (MAC Science DIP-2020K) with a monochromated Mo Kα radiation at room temperature. The structures were solved by direct methods using SHELXS-86, 97 or SIR 92 program. The refinements of structures were performed by full matrix least squares method (CRYSTAN 6.3 or SHELXL-97). The parameters were refined adopting anisotropic temperature factors for non-hydrogen atoms and isotropic ones for hydrogen atoms. The positions of hydrogen atoms were calculated by assuming a C–H bond length of 0.96 Å and sp^3 or sp^2 conformation of the carbon atoms. The temperature factors of hydrogen atoms were refined isotropically. The atomic coordinates, thermal parameters, bond lengths and angles of $(TBA)_2(TNBP)$, $(Ph_4P)_2(TNBP)$ and $(ET)_4(TNBP)$ are provided as supplementary tables. The band structure calculation was performed by the extended Hückel method with tight binding approximation and single ζ-parameter including d-orbitals of sulfur atoms.[5]

3 Results and discussion

3.1 Crystal structures of $(TBA)_2(TNBP)$ and $(Ph_4P)_2(TNBP)$§

The TBA salt of $TNBP^{2-}$ crystallizes in the monoclinic system. The lattice parameters are summarized in Table 1.

There are two kinds of $TNBP^{2-}$ molecules (A, B) having different dihedral angles (φ) between the two phenyl groups of $TNBP^{2-}$ (Fig. 3). The biphenyl system of molecule A is planar while the dihedral angle between the phenyl rings of molecule B is 35°. A similar molecular structure to that of molecule A has been observed in pristine H_2TNBP,[6] phenothiazine·H_2TNBP,[7] anthracene·H_2TNBP,[7] BEDO-TTF·H_2TNBP[2a] and $(Ph_4P)_2$-(TNBP), while the twisted form was observed in phenyl-α-naphthylamine $(H_2TNBP)_2$ ($\varphi = 38°$).[7] The coexistence of both the planar and twisted molecules in a crystal has not been observed in the H_2TNBP compounds so far. The varied molecular structures of $TNBP^{2-}$ in the TBA salt suggest the high flexibility of the molecular shape of $TNBP^{2-}$ in the formation of a solid CT complex.

§CCDC reference number 1145/203. See http://www.rsc.org/suppdata/jm/a9/a907746d for crystallographic files in .cif format.

Table 1 Crystal and refinement data for $(TBA)_2(TNBP)$, $(Ph_4P)_2(TNBP)$ and $(ET)_4(TNBP)$

	$(TBA)_2(TNBP)$	$(Ph_4P)_2(TNBP)$	$(ET)_4(TNBP)$
Crystal system	Monoclinic	Triclinic	Triclinic
Space group	$C2/c$	$P\bar{1}$	$P\bar{1}$
a/Å	42.770(3)	9.396(2)	8.691(1)
b/Å	12.461(2)	10.436(2)	12.936(1)
c/Å	19.025(1)	14.038(3)	16.208(2)
α/°		113.226(9)	97.376(9)
β/°	107.861(5)	96.24(1)	96.234(9)
γ/°		94.51(1)	103.888(9)
V/Å^3	9651(2)	1246.3(5)	1735.9(3)
Z	8	1	1
D_c/g cm^{-3}	1.168	1.390	1.820
D_o/g cm^{-3}			1.81
Diffractometer	MXC$^{\chi}$	DIP-2020K	MXC$^{\chi}$
Scan mode	2θ–ω		2θ–ω
$2\theta_{max}$/°	55	55	55
No. of intensity meas.	8938	4627	8577
Criterion for obs. Reflection	$F_0 \geqslant 4\sigma(F_0)$	$F_0 \geqslant 3\sigma(F_0)$	$F_0 \geqslant 4\sigma(F_0)$
Reflections used in L.S.	5967	2697	4906
No. of refined parameters	617	365	442
R	0.0674	0.0676	0.0656

In the TBA salt, the $TNBP^{2-}$ molecules form a segregated layer in the *ac*-plane as shown in Fig. 4a. The $TNBP^{2-}$ anion layer is sandwiched by the layers of TBA molecules (Fig. 4b) along the *b*-axis as schematically shown in Fig. 4c, where two of the alkyl chains of a TBA molecule penetrate into the anion layers, one above and one below.

$(Ph_4P)_2(TNBP)$ crystallizes in the triclinic system. The lattice parameters are summarized in Table 1. As mentioned above, only one kind of $TNBP^{2-}$ molecule, with the dihedral angle equal to 0°, is present. All the oxygen atoms of the nitro groups are out of the plane of the phenyl rings of $TNBP^{2-}$ in both TBA and Ph_4P salts.

3.2 Optical spectra of $(ET)_4(TNBP)$ and $(ET)_2(TNBP)$

The absorption spectrum of $(ET)_4(TNBP)$ (Curve a in Fig. 5) indicates strong absorptions at 3×10^3 cm^{-1} (labeled band A) and 10–11 $\times 10^3$ cm^{-1} (labeled band C) and a very weak one at 17×10^3 cm^{-1} (labeled band D). Band A, which is commonly observed in highly conductive segregated materials, is ascribed to an electronic transition either among the partially charged ET molecules or charge separated ET molecules. Band C is due to the intramolecular transition of an ET cation radical molecule (second HOMO to HOMO transition).[2,8] The weak band D is assigned to the transition from the HOMO to the LUMO of the $ET^{+\cdot}$ radical cation. Other broad absorption bands at *ca.* 20×10^3 cm^{-1} and above 30×10^3 cm^{-1} are ascribable to intramolecular transitions in the $TNBP^{2-}$ anion by comparison with those of $(TBA)_2(TNBP)$ in CH_3CN (Curve d in Fig. 5). The optical transition among the fully ionized ET

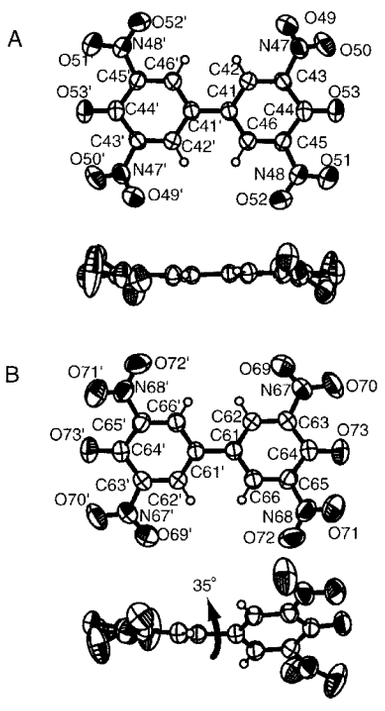

Fig. 3 Molecular structures of the two kinds of $TNBP^{2-}$ molecules (A, B) in $(TBA)_2(TNBP)$.

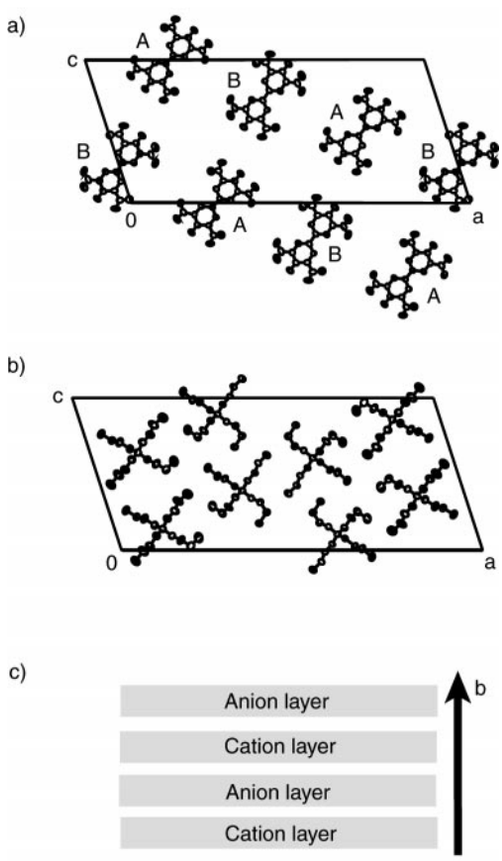

Fig. 4 Packing pattern of $TNBP^{2-}$ molecules (at $y = 0.25$) (a) and tetrabutylammonium molecules (at $y = 0.50$) (b) in the *ac*-plane. (c) represents the schematic view of the packing pattern of layers of $TNBP^{2-}$ and TBA^+.

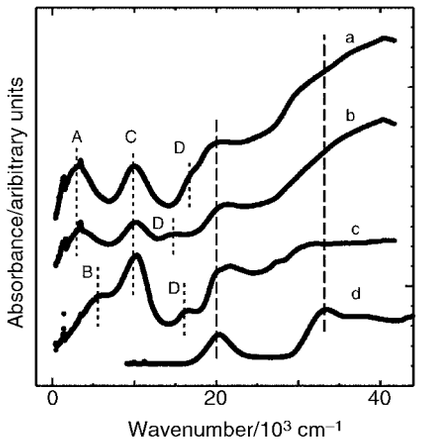

Fig. 5 Absorption spectra of $(ET)_4(TNBP)$ (a), $(ET)_2(TNBP)$ (b) and ET·Br (c) in KBr and $(TBA)_2(TNBP)$ in CH_3CN (d). For bands A, B, C and D, see text.

molecules appears at $5–6 \times 10^3$ cm^{-1} (labeled band B in curve c for ET·Br), which is not seen in curve a. Therefore all features of the absorption spectrum of the 4 : 1 complex are consistent with the segregated column composed of ET molecules having a CT degree of 1/2.

Curve b in Fig. 5 represents the absorption spectrum of $(ET)_2(TNBP)$. The spectrum clearly indicates the presence of band A and the absence of band B and all the features are very similar to those of the 4 : 1 complex. The spectrum of $(ET)_2(TNBP)$ is quite different from that expected based on its stoichiometry; namely it was expected to exhibit a similar optical spectrum to that of ET·Br which shows the characteristic lowest energy band: band B. The distinctly different appearance of the spectrum from that of ET·Br means that the charge of the ET molecules in the 2 : 1 complex is less than unity. This fact is not consistent with the chemical formula of $(ET^+)_2(TNBP^{2-})$ (Fig. 2, **V**). Since the charge of TNBP is −2, the absorption spectrum of the 2 : 1 complex shows that either the stoichiometry is not exactly 2 : 1 but the complex is anion deficient: $(ET)_2(TNBP)_{1-x}$, or the anion species are not $TNBP^{2-}$ but $[(TNBP^{2-})_{1-y}(HTNBP^-)_y]^{-2+y}$.

It is known that the intensity of band B decreases as the degree of ionicity of the ET molecule decreases from +1 in the segregated column and band B is nearly extinguished at +0.5.[9] The absence of band B in the optical spectrum of the 2 : 1 complex suggests that either x in $(ET)_2(TNBP)_{1-x}$ equals 0.5 or y in $(ET)_2(TNBP)_{1-y}(HTNBP)_y$ equals 1. The former case is completely inconsistent with the results of elemental analysis. Hence, we speculate that the $(ET)_2(TNBP)$ should be formulated as $(ET)_2(HTNBP)$ (Fig. 2, **VI**).

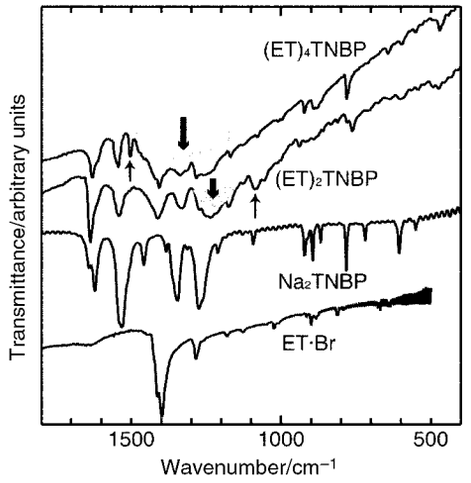

Fig. 6 IR spectra of $(ET)_4(TNBP)$, $(ET)_2(TNBP)$, $Na_2(TNBP)$ and ET·Br. The very broad band centered at around 1300 cm^{-1} in the 4 : 1 complex and a broad band at 1230 cm^{-1} in the 2 : 1 complex are indicated by thick arrows. The thin arrows indicate the band at 1504 cm^{-1} in the 4 : 1 and the band at 1087 cm^{-1} in the 2 : 1 complexes.

The IR spectra of $(ET)_4(TNBP)$ and $(ET)_2(TNBP)$ are overlapped with a broad electronic transition (band A in Fig. 5) which obscured bands which would be informative in characterizing the anion species in the 2 : 1 complex. The IR spectra of $(ET)_4(TNBP)$ and $(ET)_2(TNBP)$ in the region of 1800–400 cm^{-1} are compared with those of $Na_2(TNBP)$ and ET·Br in Fig. 6. In general each band of the 4 : 1 and 2 : 1 complexes is assignable to those of ET·Br and $Na_2(TNBP)$. Even though the 4 : 1 and 2 : 1 complexes have similar features, it is quite apparent that the 2 : 1 complex is not contaminated with the 4 : 1 complex. There is a very broad band centered at around 1300 cm^{-1} only in the 4 : 1 complex (indicated by thick arrow in Fig. 6). It is known that the aν_4 mode of $ET^{+\cdot}$ appearing at 1300 cm^{-1} (ref. 10) is a parameter of the magnitude of electron–molecular vibration (e–mv) coupling. No such band, but a broad band at 1230 cm^{-1} (indicated by thick arrow), was observed in the 2 : 1 complex. The appearances of bands at 1504 cm^{-1} in the 4 : 1 complex and at 1087 cm^{-1} in the 2 : 1 complex (indicated by thin arrows) allows clear discrimination between the two complexes.

The band at 1330–1338 cm^{-1} is assignable to the a_g mode of $ET^{+\cdot}$. The appearance of this band indicates lattice distortion such as dimerization of ET molecules in the segregated layer.

3.3 Molecular and crystal structures of $(ET)_4(TNBP)$

The $(ET)_4(TNBP)$ complex crystallizes in the triclinic system and its lattice parameters are summarized in Table 1. The ET molecules form a two-dimensional segregated layer in the *ab*-plane which is sandwiched by the layers of $TNBP^{2-}$ molecules (Fig. 7). There are two crystallographically independent ET molecules (A, B) and they stack in the sequence BAAB to form a tetramer along the *a*-axis. The interplanar distances between BA, AA, AB, and BB are 3.66, 3.67, 3.67 and 3.77 Å, respectively. The $TNBP^{2-}$ molecules are located close to the *ab*-plane as seen in Fig. 7b. Fig. 8 shows the molecular structures of the ET and $TNBP^{2-}$ molecules. The TNBP molecule is planar as far as the biphenyl moiety is concerned. Although the nitrogen atoms of the nitro groups and the phenolate oxygen atoms are in the plane of the biphenyl moiety, the oxygen atoms of nitro groups deviate from the plane by 0.99 Å. The ethylene groups of the ET molecules are in a staggered configuration. According to the relation proposed between the degree of CT and the bond lengths of the ET molecule,[11] charges of +0.52 and +0.62 were estimated for molecules A and B, respectively, while the plots of bond lengths of the ET molecule against the degree of CT[12] gave the average charge of $+0.50 \pm 0.14$ and $+0.57 \pm 0.25$ for molecules A and B, respectively. As a consequence, it is reasonably concluded that every ET molecule has a CT degree of +1/2.

There are short O···H atomic contacts less than the sum of the van der Waals radii (2.72 Å) between the ethylene hydrogens of the ET molecules and the oxygen atoms of the nitro group or biphenolate as shown by the dotted lines in Fig. 7c. Some sort of CH···O interaction has been adopted such as a hydrogen bond, where the C···O distance is less than 3.0–4.0 Å (*cf.* the sum of the van der Waals radii of O and H atoms and covalent radius of CH = 3.82 Å).[13] We have observed that the short CH···O contacts (C···O 3.41–3.55 Å) gave rise to the cohesive interaction in many metallic BEDO-TTF complexes.[2a]

The lengths of the CH···O bonds between the ET molecules and $TNBP^{2-}$ molecules are summarized in Table 2. The molecule A has two short CH···O atomic contacts (shown by contacts (1) and (2) in Fig. 7c), while the molecule B has six

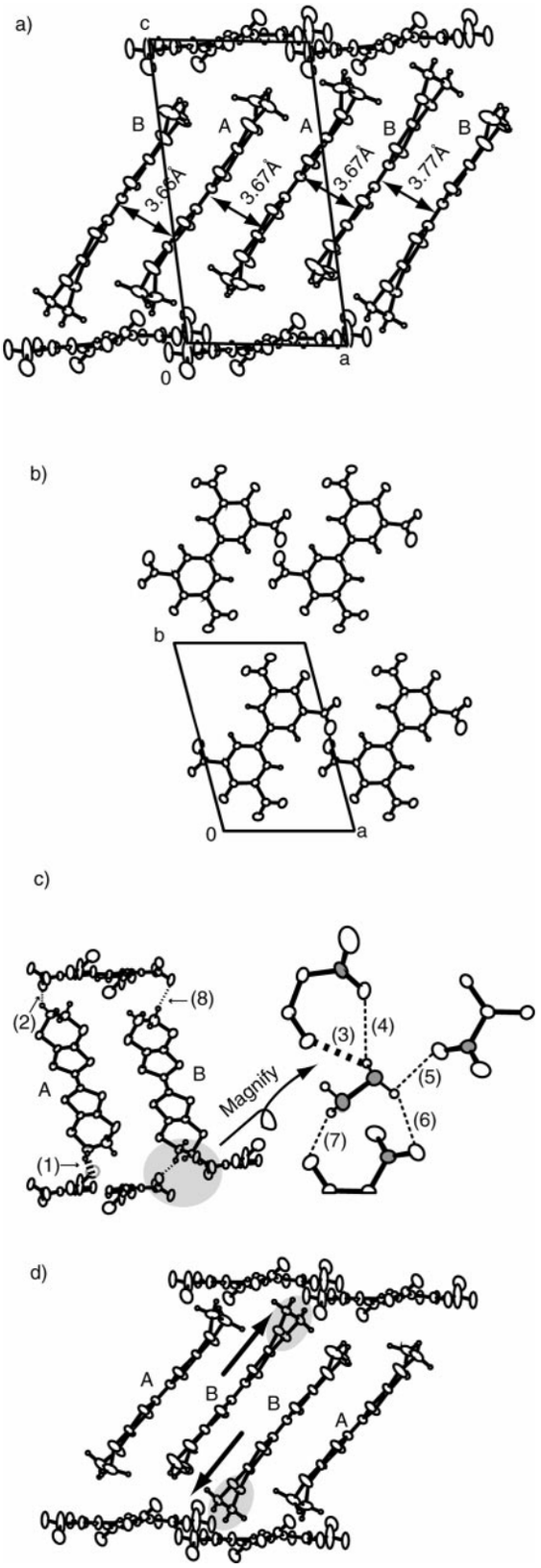

Fig. 7 Crystal structure of $(ET)_4(TNBP)$. A and B represent two crystallographically independent ET molecules. (a) The *b*-axis projection of a donor column along $a+0.5b$ direction and the anion layer. Other ET molecules were omitted for simplicity. (b) The *c*-axis projection of an anion layer. (c) View of the intermolecular CH···O contacts (thick dotted lines <2.5 Å, thin ones >2.5 Å). Left, a pair of neighboring ET molecules in the side-by side direction and the anion molecules viewed along the *a*-axis are depicted. The shaded part was magnified and projected onto the *ab*-plane (right) (the ethylene carbon atoms of ET and nitrogen atoms of $TNBP^{2-}$ were shaded). (d) A donor column and the anion molecules were projected along the *b*-axis. The shaded areas indicate the spaces in which the distinct CH···O contacts were observed.

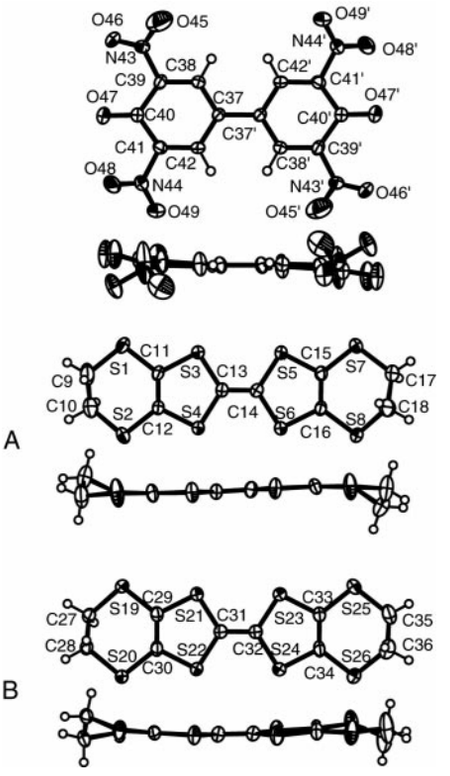

Fig. 8 Molecular structures of $TNBP^{2-}$ and ET molecules in $(ET)_4(TNBP)$ (from top to bottom). Each molecule was projected onto the molecular plane (upper) and along the molecular transverse axis (lower). Notations of A and B for ET molecules correspond to those in Fig. 7.

such contacts (contacts (3)–(8) in Fig. 7c). Among them five short contacts ((3)–(7) in Fig. 7c) are centered at one methylene group at one side of the ET molecule (B) as depicted in the enlarged figure of Fig. 7c. Such a hydrogen bond may be the main cause of the formation of the tetramer of ET molecules as depicted in Fig. 7d. The shaded parts in Fig. 7 represent the places where short CH···O contacts are centered.

The stacking pattern of the ET molecules is the β″-type with the overlap integrals summarized in Fig. 9 and Table 3. According to the classification of the stacking pattern of ET molecules proposed by Mori,[14] this system is denoted as a β''_{432}-type, which is so far unknown. The formation of the unique β″-type structure in the 4 : 1 complex is ascribable to the short CH···O hydrogen bonds between the different kinds of layers and the resultant small dihedral angles between the ET molecular planes and the anion layers (50 and 52° *vs.* 63° for β''_{420} ($(ET)_2$(MeO-TCA)[15]) and 78° for β''_{412} ($(ET)_2$(PrO-TCA)[15]).

Based on the crystal structure at room temperature, the energy dispersion, density of states and the Fermi surface were calculated by the extended Hückel method as shown in

Table 2 Distances of CH···O hydrogen bonds between $ET^{0.5+}$ and $TNBP^{2-}$ molecules in $(ET)_4(TNBP)$

	Atom names	*d*(H···O)/Å	*d*(C···O)/Å
(1)	C10-H10B···O45	2.43(9)	3.25(1)
(2)	C18-H18B···O49	2.65(9)	3.32(1)
(3)	C27-H27B···O48	2.36(8)	3.052(9)
(4)	C27-H27B···O46	2.67(8)	3.375(9)
(5)	C27-H27B···O49	2.70(8)	3.099(9)
(6)	C27-H27B···O49′	2.56(9)	3.423(9)
(7)	C28-H28B···O47	2.54(8)	3.449(9)
(8)	C35-H35B···O48	2.64(9)	3.58(1)

Positions of hydrogen atoms are calculated by assuming sp^3 C–H bond of 0.96 Å. Bonds (1)–(8) are shown in Fig. 7.

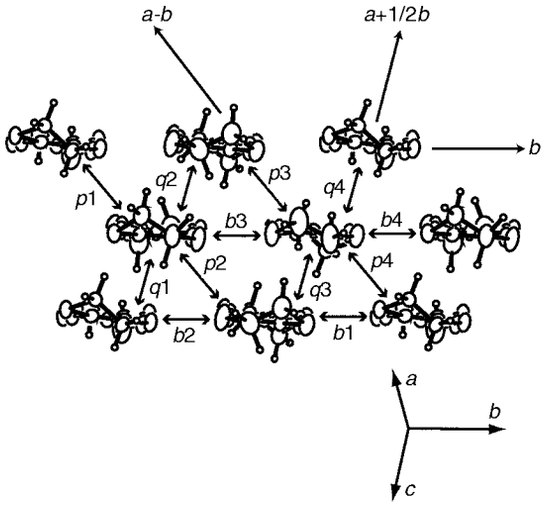

Fig. 9 Packing pattern of ET molecules and the notation of overlap integrals in $(ET)_4(TNBP)$. See Table 3 for calculated overlap integrals.

Fig. 10.[16] The four HOMO orbitals of the ET molecules compose the wide conduction band with bandwidth of 0.94 eV. There is no band splitting in the HOMO band. The calculated density of states at the Fermi level, DOS (ε_F), is 0.90 states eV^{-1} $molecule^{-1}$ $spin^{-1}$, which is comparable to those of κ-$(ET)_2X$ (X = $Cu(NCS)_2$, $Cu[N(CN)_2]Cl$, I_3) and β-$(ET)_2IBr_2$.[3] There are two kinds of closed Fermi surfaces, one positive at around C and the other negative near Y indicating the semimetallic nature of the compound.

3.4 Electrical conductivity and magnetic susceptibility

3.4.1 4 : 1 Complex. The room temperature electrical conductivity of $(ET)_4(TNBP)$ in the *ab*-plane was 50–80 S cm^{-1}. It showed metallic behavior all the way down to 3 K ($\sigma_{3\,K} = 2.8 \times 10^3$ S cm^{-1}), frequently with a resistivity jump due to cracking in the crystal at 50–70 K (Fig. 11). No cooling rate dependence was noticed. The resistivity followed approximately the T^2 dependence of eqn. (1) in the whole temperature region measured as shown in the inset of Fig. 11.

$$\rho = 1.63 \times 10^{-7} T^2 + 7.73 \times 10^{-4} \quad (1)$$

Therefore, the 4 : 1 complex is a good metal in spite of the calculated semimetallic Fermi surface, that is similar to the case of $(ET)_2ClO_4(TCE)_{0.5}$.[17]

EPR measurements were performed on the 4 : 1 complex with alignment of the external magnetic field H_0 and crystal as depicted in Fig. 12. The angle dependences of the *g* values and the line-width (peak-to-peak; ΔH) of the complex at room temperature exhibited a phase difference of *ca.* 30° in Fig. 12a. H_0 is parallel to the *c**-axis (or perpendicular to the conducting plane) at 120°. This is the alignment where a Dysonian signal has the smallest peak height ratio (*A*/*B*). The *A*/*B* value of the Dysonian signal was constant down to about 60 K (*A*/*B* = 1.01–1.03) followed by a slight increase to *A*/*B* = 1.08 at about 10 K (Fig. 13a). Accordingly, to obtain the EPR parameters the signal was analyzed assuming a Lorentzian signal in this

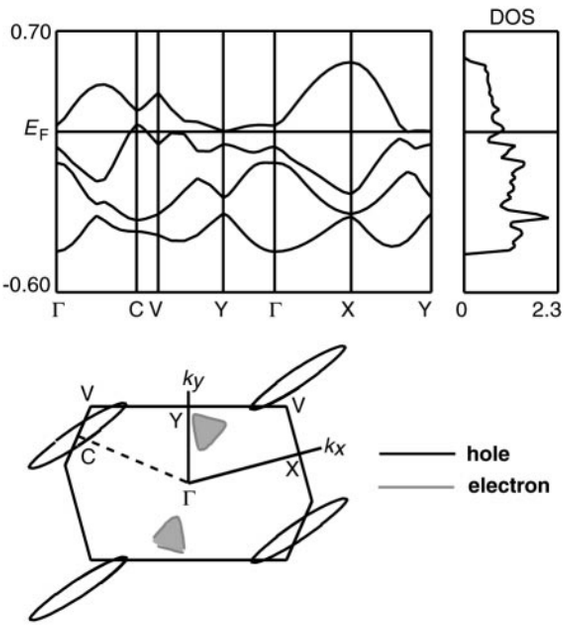

Fig. 10 Energy dispersion, density of states and Fermi surfaces of $(ET)_4(TNBP)$ calculated by extended Hückel method with tight binding approximation and single ζ-parameter including d-orbitals of sulfur, atoms of ET molecules.[6] Electronic pockets are shaded.

configuration. Hence, the EPR parameters below 60 K, as described in the following, have a slight ambiguity.

When H_0 is normal to the *c**-axis (or parallel to the conducting layer, Fig. 12b), the angle dependences of the *g* values and the line-width are in phase and a typical Dysonian signal survives. The *A*/*B* value of the Dysonian signal exhibited a nearly constant value of 1.2 from RT to 120 K followed by a gradual increase down to 40 K (1.4–1.6) and a rapid one below it (1.9–2.2 at 4 K). The *g* values at RT were *ca.* 2.0080, *ca.* 2.0062 and *ca.* 2.0042 along the *c**, *b* and *a*-axes, respectively (Fig. 12), in good accordance with the molecular orientation of the ET molecule in the crystal.[18] The magnitudes of the ΔH values are similar to or a little less than those of β″-$(ET)_2X$ (X = $AuBr_2$, IAuBr).[19,20]

When H_0 is parallel to the *c**-axis, the *g* values exhibited a very slight temperature dependence down to low temperatures as shown in Fig. 13b ($g = 2.0078$–2.0081) indicating no orientational change of the ET molecules.

ΔH shows a steady decrease with decreasing temperature, as shown in Fig. 13c, which is in accordance with the temperature dependence of resistivity. This kind of behavior has been observed in several metallic ET compounds[18,19,21] suggesting that an Elliott-like mechanism is applicable for the conduction electrons in this system.[22] The temperature dependence of ΔH is a function of neither T nor T^2. The line width between 150 K and 20 K is well approximated by a smooth function of $T^{1/2}$ and no anomaly was detected. Even though the mechanism of the $T^{1/2}$ dependence of ΔH is not clear, it can be said, based on the temperature dependences of the *g* and ΔH values, that no magnetic phase transition took place down to 4 K in this complex.

Although the material exhibited a metallic temperature dependence in its electrical resistivity (Fig. 11) as well as in its

Table 3 Calculated overlap integrals ($\times 10^{-3}$)

	Overlap integral		Overlap integral		Overlap integral
*b*1	8.1	*p*1	17.7	*q*1	−3.2
*b*2	8.4	*p*2	15.9	*q*2	−3.9
*b*3	8.4	*p*3	17.7	*q*3	−3.2
*b*4	8.1	*p*4	9.2	*q*4	−4.4

*b*1–*b*4, *p*1–*p*4 and *q*1–*q*4 are defined in Fig. 9.

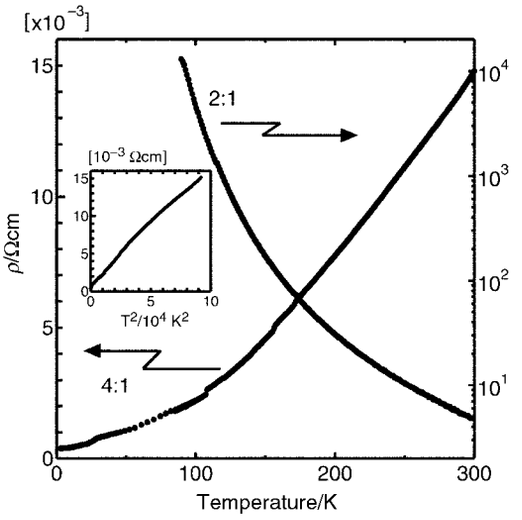

Fig. 11 Temperature dependence of resistivity of $(ET)_4(TNBP)$ (single crystal) and $(ET)_2(TNBP)$ (pellet sample). The inset shows the T^2 dependence of resistivity of $(ET)_4(TNBP)$.

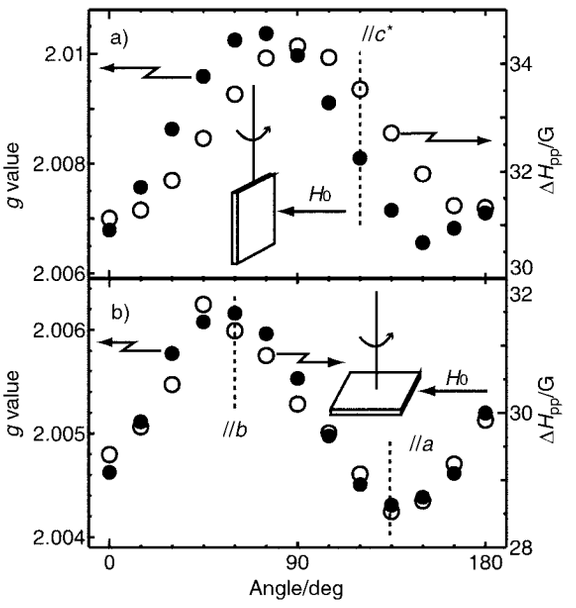

Fig. 12 Angle dependence of the g value and peak-to-peak line-width (ΔH) of $(ET)_4(TNBP)$. The alignment of external magnetic field and the crystal is depicted in the figure. a) H_0 is parallel to the c*-axis at 120°. b) H_0 is perpendicular to the c*-axis.

EPR line width (Fig. 13c), the spin susceptibility showed a monotonic decrease with lowering temperature down to *ca.* 40 K followed by an increase due to Curie impurity (Fig. 13d). That is quite different from those of the metallic ET complexes having large Fermi surfaces, where the spin susceptibility is insensitive to temperature.[18,19,21] The temperature dependence of spin susceptibility by EPR measurement was confirmed by the following SQUID measurement.

The magnetic susceptibility measured by SQUID exhibited a weakly temperature dependent susceptibility down to 35 K followed by a rapid increase. The rapid increase of susceptibility below 35 K was ascribable to Curie impurity with a Curie constant of 9.55×10^{-4} emu K fu^{-1} (fu = $(ET)_4(TNBP)$) which corresponds to a spin amount of 0.025% of fu. The subtraction of Curie impurity gave Fig. 14. The susceptibility at RT was 1.33×10^{-3} emu mol^{-1} which is equal to 6.7×10^{-4} emu mol^{-1} for one ET spin. This value is a little smaller than that obtained by an EPR measurement (χ_{spin} (RT) = 1.5×10^{-3} emu mol^{-1}). This value is fairly high compared with those of good metals among the ET organic metals ($3.4–4.6\times10^{-4}$ emu mol^{-1} for β-$(ET)_2X$, X = AuI_2,[23] I_3[24]) and even with those of the 10 K class ET superconductors ($4.5–5.5\times10^{-3}$ emu mol^{-1} for κ-$(ET)_2X$, X = $Cu(NCS)_2$,[25] $Cu(CN)[N(CN)_2]$,[25] $Cu[N(CN)_2]Br$,[25] $Cu[N(CN)_2]Cl$[26]), which are known to have rather strong electron correlation. The susceptibility is close to those of the Mott insulators of ET materials ($7.1–9.6\times10^{-4}$ emu mol^{-1} for β′-$(ET)_2AuCl_2$,[27] β′-$(ET)_2ICl_2$,[28] κ-$(ET)_2Cu_2(CN)_3$[29]). Therefore, as far as the magnetic susceptibility is concerned, this system is thought to have a large enhancement factor due to strong electron correlation.

The susceptibility decreased to 2/3 of the RT value with decreasing temperature; 8.8×10^{-4} emu mol^{-1} below 50 K. The decrease of susceptibility is more intense than those of the 10 K class ET superconductors which show a 10–20% decrease.[25,26] The strong temperature dependence of susceptibility is reminiscent of those of $(ET)_4M(CN)_4H_2O$ (M = Ni, Pd, Pt) which have a semimetallic small Fermi surface.[30]

Using the calculated density of states at Fermi level: $D(\varepsilon_F)$ = 0.90 states eV^{-1} molecule^{-1} spin^{-1}, susceptibility with no enhancement: $\chi_{Pauli}^{(0)}$ was calculated as 0.58×10^{-4} emu mol^{-1} according to eqn. (2).

$$\chi_{Pauli}^{(0)} = g^2\mu_B^2 D(\varepsilon_F) \quad (2)$$

Using this value, the effective on-site Coulomb repulsive energy U_{eff} of 1.06 ± 0.01 eV from RT to below 50 K was evaluated based on eqn. (3).

$$\chi_{Pauli}^{obs} = \chi_{Pauli}^{(0)}/\{1 - U_{eff}D(\varepsilon_F)\} \quad (3)$$

These U_{eff} values are nearly the same as or a little smaller than those of the 10 K class ET superconductors having strong electron correlation; κ-$(ET)_2X$ (U_{eff} = 1.0 eV for X = $Cu[N(CN)_2]Br$, 1.2 eV for $Cu[N(CN)_2]Cl$).[26] It is noteworthy that the 4 : 1 complex has a band width comparable to

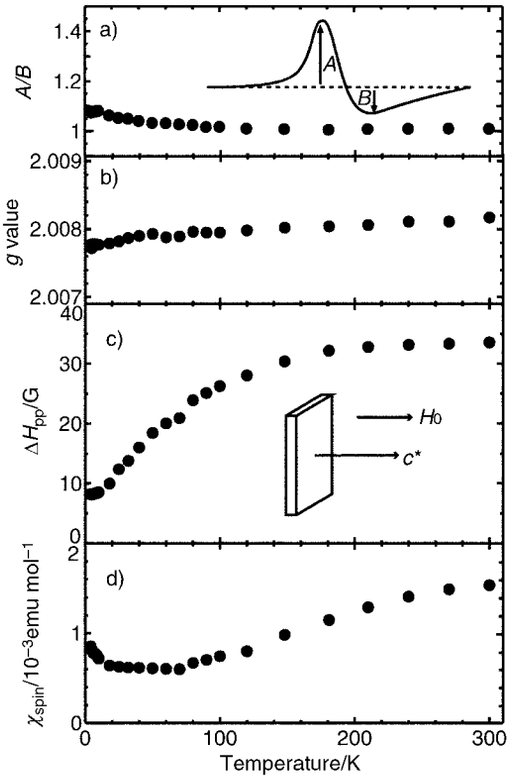

Fig. 13 Temperature dependence of the A/B, g value, line-width (ΔH) and spin susceptibility (χ_{spin}) of $(ET)_4(TNBP)$ when $H_0//c$*.

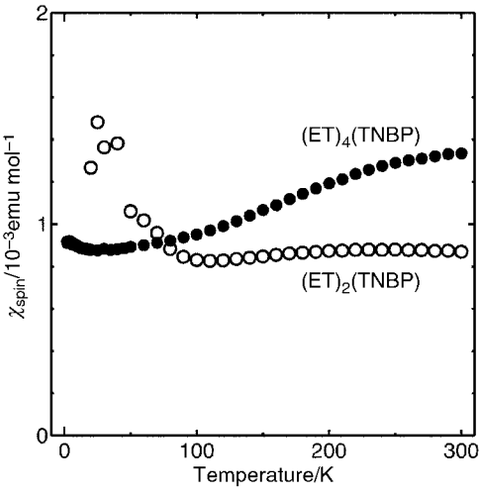

Fig. 14 Magnetic susceptibility of $(ET)_4(TNBP)$ and $(ET)_2(TNBP)$ by SQUID after correction of Curie impurity.

the magnitude of the effective on-site Coulomb repulsive energy.

The strong temperature dependence of susceptibility even in the metallic region for the ET complexes of TNBP as well as $M(CN)_4{\cdot}H_2O$[30] may be ascribable to the fact that they have semimetallic Fermi surfaces with a small area.

3.4.2 2 : 1 Complex. In accordance with the optical spectrum in Fig. 5, the 2 : 1 complex is highly conductive. The room temperature conductivity of the pellet sample of $(ET)_2(TNBP)$ was 0.2 S cm^{-1} and a semiconductive behavior was observed with the activation energy of 89 meV down to 90 K (Fig. 11). This result strongly supports the theory that the formula of this 2 : 1 salt is not $(ET^{1+})_2(TNBP^{2-})$, which eventually corresponds to an insulating CT degree according to Mott criterion.

The magnetic susceptibility measured by SQUID exhibited weakly temperature dependent susceptibility down to 20 K followed by a rapid increase. The rapid increase of susceptibility below 20 K was ascribable to Curie impurity with Curie constant of 1.61×10^{-2} emu K fu^{-1} (fu = $(ET)_2(TNBP)$, between 20 and 2.2 K) which corresponds spin amount of 0.43% of fu. The magnitude of Curie impurity is rather high compared with that in the 4 : 1 complex.

The temperature dependence of spin susceptibility shown in Fig. 14 is after the correction of Curie impurity where the data below 20 K are eliminated due to large scattering. The susceptibility at RT was 8.2×10^{-4} emu mol^{-1}, high enough for a strongly correlated spin system of $ET^{0.5+}$ compounds.[27–29] A gradual increase of susceptibility is seen down to 20 K. It is most plausible that this system has Bonner–Fisher type antiferromagnetic interactions.

The appearances of band A (3×10^3 cm^{-1}) and a_g mode (1330–1338 cm^{-1}) in the UV–VIS–NIR and IR spectra indicate that the complex has a non-uniform segregated stack or layer having a uniform partial CT state. The electrical conductivity and magnetic data suggest that the lattice distortion (probably dimerization) causes the localization of electrons (one electron per dimer) but the localization is not strong enough to extinguish the carrier. That is reminiscent of that of the highly conductive Mott insulator $ET^{0.5+}$ system; κ-$(ET)_2Cu_2(CN)_3$ (σ_{RT} = 10–20 S cm^{-1}, ε_a = 20–50 meV, $\chi_{spin} = 8 \times 10^{-4}$ emu mol^{-1}).[29,31] However, without information on crystal and molecular structures, no further interpretation of magnetic and transport properties can be made including both the increase of susceptibility down to 20 K and the mechanism of formation of the complex having the postulated formula: $(ET^{0.5+})_2(HTNBP^{1-})$ (Fig. 2, **VI** instead of **V**).

4 Summary

Crystal structures of $TNBP^{2-}$ complexes with tetrabutylammonium (2 : 1), tetraphenylphosphonium (2 : 1), and BEDT-TTF(ET) (4 : 1) were determined. Two kinds of molecular structures of the $TNBP^{2-}$ molecule were found indicating the flexible nature of the $TNBP^{2-}$ molecule. The 4 : 1 ET complex is a metal where flexible $TNBP^{2-}$ molecules form flat anion layers. The $ET^{+0.5}$ molecules construct a unique β''_{432}-type packing which is mainly created by the CH···O hydrogen bonds. A semimetallic nature is suggested from the temperature dependence of the magnetic susceptibility and the band structure based on the extended Hückel method. The calculated band width is comparable to the estimated effective on-site Coulomb repulsive energy. The 4 : 1 ET complex is regarded as a metal having a highly correlated spin system. A nearly 2 : 1 complex of ET was also obtained. Its highly conductive nature and optical absorption spectrum clearly indicated that the counter anion in this complex is not $TNBP^{2-}$ but plausibly $HTNBP^{-}$. The magnetic properties suggest strong electron correlation.

Acknowledgements

This work was in part supported by a Grant-in-Aid for Scientific Research from the Ministry of Education, Science, Sports, and Culture, Japan, a Grant for CREST (Core Research for Evolutional Science and Technology) of Japan Science and Technology Corporation (JST) and a fund for "Research for for Future" from Japan Society for Promotion of Science.

References

1 G. Saito and Y. Matsunaga, *Bull. Chem. Soc. Jpn.*, 1973, **46**, 1609.
2 (*a*) S. Horiuchi, H. Yamochi, G. Saito, K. Sakaguchi and M. Kusunoki, *J. Am. Chem. Soc.*, 1996, **118**, 8604; (*b*) T. Senga, K. Kamoshida, L. A. Kushch, G. Saito, T. Inayoshi and I. Ono, *Mol. Cryst. Liq. Cryst.*, 1997, **296**, 97.
3 T. Ishiguro, K. Yamaji and G. Saito, *Organic Superconductors*, 2nd edn., Springer, Berlin, 1998.
4 E. Kunze, *Ber. Dtsch. Chem. Ges.*, 1888, **21**, 3331.
5 T. Mori, A. Kobayashi, Y. Sasaki, H. Kobayashi, G. Saito and H. Inokuchi, *Bull. Chem. Soc. Jpn.*, 1984, **57**, 627.
6 Z. A. Starikova, T. M. Shchegoleva, V. K. Trunov, O. B. Lantratova and I. E. Pokrovskaya, *Zh. Strukt. Khim.*, 1979, **20**, 514.
7 K. Nishimura, MSc Thesis, 1999, Kyoto University.
8 (*a*) O. O. Drozdova, V. N. Semkin, R. M. Vlasova, N. D. Kushch and E. B. Yagubskii, *Synth. Met.*, 1994, **64**, 17; (*b*) T. Hasegawa, S. Kagoshima, T. Mochida, S. Sugiura and Y. Iwasa, *Solid State Commun.*, 1997, **103**, 489.
9 T. Sugano, K. Yakushi and H. Kuroda, *Bull. Chem. Soc. Jpn.*, 1978, **51**, 1041.
10 (*a*) M. Meneghetti, R. Bozio and C. Pecile, *J. Phys. (Paris)*, 1986, **47**, 1377; (*b*) K. I. Pokhodnia, E. M. Kozlov, V. G. Onischenko, D. Schweitzer, J. Moldenhauer and R. Zamboni, *Synth. Met.*, 1993, **55–57**, 2364.
11 P. Guionneau, C. J. Kepert, D. Chasseau, M. R. Truter and P. Day, *Synth. Met.*, 1997, **86**, 1973.
12 G. Saito, H. Izukashi, M. Shibata, K. Yoshida, L. A. Kushch, T. Kondo, H. Yamochi, O. O. Drozdova, K. Matsumoto, M. Kusunoki, K. Sakaguchi, N. Kojima and E. B. Yagubskii, *J. Mater. Chem.*, submitted.
13 (*a*) G. R. Desiraju, *Acc. Chem. Res.*, 1991, **24**, 290; (*b*) Y. Gu, T. Kar and S. Scheiner, *J. Am. Chem. Soc.*, 1999, **121**, 9411.
14 T. Mori, *Bull. Chem. Soc. Jpn.*, 1998, **71**, 2509.
15 (*a*) H. Yamochi, C. Tada, S. Sekizaki, G. Saito, M. Kusunoki and K. Sakaguchi, *Mol. Cryst. Liq. Cryst.*, 1996, **284**, 379; (*b*) S. Sekizaki, H. Yamochi and G. Saito, *Synth. Met.*, 1999, **102**, 1711.
16 The band structures calculated by the extended Hückel method differ considerably in their ζ-parameters and whether it includes 3d-orbital of sulfur atoms or not: both the hole-like and electron-like closed Fermi surfaces are obtainable by the methods of

T. Mori *et al.* (ref. 5, single ζ, including 3d, Fig. 10 in this paper), R. Ramakumar, Y. Tanaka and K. Yamaji, *Phys. Rev. B*, 1997, **56**, 795, single ζ, excluding 3d, and M.-H.Whangbo, J. M. Williams, P. C. W. Leung, M. A. Beno, T. J. Emge and H. H. Wang, *Inorg. Chem.*, 1985, **24**, 3500, double ζ, excluding 3d, though the shapes of the corresponding Fermi surfaces are different to each other; no Fermi surfaces were obtainable by the methods of A. J. Berlinsky, J. F. Carolan and L. Weiler, *Solid State Commun.*, 1974, **15**, 795, double ζ, including 3d; quasi-one-dimensional Fermi surfaces are obtained by the method of R. Kato, Y.-L. Liu, H. Sawa, S. Aonuma, A. Ichikawa, H. Takahashi and N. Mori, *Solid State Commun.*, 1995, **94**, 973, single ζ, excluding 3d.

17 (*a*) G. Saito, T. Enoki, K. Toriumi and H. Inokuchi, *Solid State Commun.*, 1982, **42**, 557; (*b*) G. Saito, T. Enoki, H. Inokuchi and H. Kobayashi, *J. Phys. (Paris)*, 1983, **44**, C3–1215; (*c*) M. Kobayashi, T. Enoki, K. Imaeda, H. Inokuchi and G. Saito, *Phys. Rev. B*, 1987, **36**, 1457.

18 T. Sugano, G. Saito and M. Kinoshita, *Phys. Rev. B*, 1986, **34**, 117.

19 M. Kurmoo, D. R. Talham, P. Day, I. D. Parker, R. H. Friend, A. M. Stringer and J. A. K. Howard, *Solid State Commun.*, 1987, **61**, 459.

20 A. Ugawa, Y. Okawa, K. Yakushi, H. Kuroda, A. Kawamoto, J. Tanaka, K. Murata and T. Ishiguro, *Synth. Met.*, 1988, **27**, A407.

21 (*a*) E. L. Venturini, L. J. Azevedo, J. E. Shirber, J. M. Williams and H. H. Wang, *Phys. Rev. B*, 1985, **32**, 2819; (*b*) T. Sugano, G. Saito and M. Kinoshita, *Phys. Rev. B*, 1987, **35**, 6554; (*c*) M. Oshima, H. Mori, G. Saito and K. Oshima, *The Physics and Chemistry of Organic Superconductors*, eds. G. Saito and S. Kagoshima, Springer-Verlag, Berlin, 1990, p. 257.

22 R. J. Elliott, *Phys. Rev.*, 1954, **96**, 266.

23 D. R. Talham, K. Kurmoo, P. Day, D. S. Obertelli, I. D. Parker and R. H. Friend, *J. Phys. C*, 1986, **19**, L383.

24 B. Rothaemel, L. Forro, J. R.Cooper, J. S. Schilling, M. Weger, P. Bele, H. Brunner, D. Schweitzer and H. J. Keller, *Phys. Rev. B*, 1986, **34**, 704.

25 T. Nakamura, T. Nobutoki, T. Takahashi, G. Saito, H. Mori and T. Mori, *J. Phys. Soc. Jpn.*, 1994, **63**, 4110.

26 M. Kubota, G. Saito, H. Ito, T. Ishiguro and N. Kojima, *Mol. Cryst. Liq. Cryst.*, 1996, **284**, 367.

27 T. Mori and H. Inokuchi, *Solid State Commun.*, 1987, **62**, 525.

28 M. Tokumoto, H. Anzai, T. Ishiguro, G. Saito, H. Kobayashi, R. Kato and A. Kobayashi, *Synth. Met.*, 1987, **19**, 215.

29 T. Komatsu, N. Matsukawa, T. Inoue and G. Saito, *J. Phys. Soc. Jpn.*, 1996, **65**, 1340.

30 (*a*) H. Mori, I. Hirabayashi, S. Tanaka, T. Mori, Y. Maruyama and H. Inokuchi, *Solid State Commun.*, 1991, **80**, 411; (*b*) T. Mori, K. Kato, Y. Maruyama, H. Inokuchi, H. Mori, I. Hirabayashi and S. Tanaka, *Solid State Commun.*, 1992, **82**, 177.

31 U. Geiser, H. H. Wang, K. D. Carlson, J. M. Williams, H. A. Charlier Jr., J. E. Heindl, G. A. Yaconi, B. H. Love, M. W. Lathrop, J. E. Schirber, D. L. Overmyer, J. Ren and M.-H. Whangbo, *Inorg. Chem.*, 1991, **30**, 2586.

Paper a907746d